Journal of Building Engineering 44 (2021) 103264

Contents lists available at ScienceDirect

Journal of Building Engineering

journal homepage: www.elsevier.com/locate/jobe

Mechanical and durability properties of ultra-high performance steel FRC made with discarded materials

Abdelrahman Abushanab [a], Wael Alnahhal [b,*], Muazzam Ghous Sohail [c], Nasser Alnuaimi [d], Ramazan Kahraman [e], Nezam Altayeh [a]

[a] Department of Civil and Architectural Engineering, Qatar University, Doha, Qatar
[b] Department of Civil and Architectural Engineering, College of Engineering, Qatar University, Doha, Qatar
[c] Center for Advanced Materials, Qatar University, Doha, Qatar
[d] Department of Civil and Architectural Engineering, Qatar University, Qatar
[e] Department of Chemical Engineering, Qatar University, Doha, Qatar

ARTICLE INFO

Keywords:
Steel slag aggregate
Recycled concrete aggregate
Ultra-high performance concrete
Fiber reinforced concrete
Durability
Steel fibers

ABSTRACT

This study investigates the mechanical and durability properties of 12 ultra-high performance fiber reinforced concrete (UHPFRC) mixes manufactured using alternate aggregate sources. Natural gabbro aggregates (GA), steel slag aggregates (SSA), and recycled concrete aggregates (RCA) were employed as coarse aggregates. The volume of the coarse aggregates was limited to 12.5% of the total UHPC volume. Three types of steel fibers were employed: macro hooked-end fibers, micro straight fibers, and a hybrid combination of these two fibers. The fiber volume fractions tested were 0% and 1%. Properties investigated were compressive and flexural tensile strengths, electrical resistivity, porosity, and rapid chloride permeability. Test results revealed that the effect of aggregate type was more pronounced on the flexural strength than compressive strength. UHPFRC with steel micro-fibers or a hybrid combination of both steel macro and micro-fibers had a more noticeable effect on the compressive strength than that with steel macro-fibers, irrespective of aggregate type. Moreover, UHPFRC specimens with steel macro-fibers showed the highest flexural strength, regardless of the aggregate type. The SSA improved all durability properties of UHPFRC, whereas RCA noticeably deteriorated the resistivity and chloride permeability. The incorporation of steel micro-fibers improved the porosity and chloride permeability of all UHPFRC mixes.

1. Introduction

Concrete plays a significant role in the construction industry, from small structures to major monuments and facilities that promote national visions and identities. The annual production of concrete is currently estimated at 9 billion tons worldwide, and this figure is projected to rise to 18 billion tons by 2050, raising concerns regarding the greenhouse gas emissions and depletion of natural aggregates (NA) in most parts of the world [1]. In fact, concrete production accounts for approximately 10% of total CO_2 emissions in the environment [2]. Moreover, the annual global demand for NA is currently 40 billion tons and is expected to increase to 66 billion tons by 2025 [3]. Hence, there is a substantial need to utilize recycled materials and industrial by-products for concrete applications.

Construction and demolition (C&D) waste has recently been proposed as a promising alternative to NA. The annual worldwide generation of C&D waste reached 3 billion tons in 2018 [4]. Of the 3 billion tons of C&D waste, 66 million tons are annually generated in the Gulf Cooperation Council (GCC) countries [5]. Converting such waste to recycled concrete aggregates (RCA) reduces the depletion of NA, total cost of concrete, CO_2 emissions, and C&D waste disposal cost [6–9]. Numerous studies investigated the effect of incorporating RCA in normal-strength concrete (NSC) and high-performance concrete (HPC). Huda and Alam [10] and Kurda et al. [11] found that the slump of RCA concrete decreased as the replacement ratio of RCA increased. Alnahhal and Aljidda [12] and Kumar et al. [13] suggested that RCA should be in a saturated surface dry condition (SSD) before mixing to avoid concrete slump loss. Dimitriou et al. [14] and Younis et al. [15] observed that 100% RCA concrete had a 20–50% lower compressive strength than conventional concrete. A similar observation was also reported in the

* Corresponding author.
E-mail address: wael.alnahhal@qu.edu.qa (W. Alnahhal).

https://doi.org/10.1016/j.jobe.2021.103264
Received 17 May 2021; Received in revised form 29 August 2021; Accepted 5 September 2021
Available online 9 September 2021

literature [2,6,12,16–19]. In addition, Wagih et al. [16] and Wang et al. [20] reported that the concrete modulus of rupture was decreased by 20% at a 100% RCA replacement ratio. Thomas et al. [21] noticed that 100% RCA concrete exhibited 7%–19% lower splitting tensile strength than conventional concrete. Verma and Ashish [22] recognized that the mechanical properties of RCA concrete were comparable to conventional concrete when the RCA replacement ratio was limited to 50%. Regarding the influence of RCA on the durability properties of concrete, De Brito et al. [23] observed that the incorporation of RCA increased the corrosion susceptibility of reinforced concrete structures. Ali et al. [24] reported that the water absorption and chloride penetration of 100% RCA concrete were 21% and 43% higher than that of conventional concrete, respectively. Andreu and Miren [25] and Thomas and et al. [26] have also observed similar results. Furthermore, Andreu and Miren [25] found that RCA should be produced from a 60 MPa compressive strength concrete to achieve comparable mechanical properties to conventional HPC concrete. Moreover, the authors found that a 50% RCA replacement ratio had no effect on the durability properties of HPC.

Likewise, steel slag aggregates (SSA) are another alternative to NA for concrete applications. It is estimated that the global production of steel slag is as high as 250 million tons per year, of which 400,000 tons are annually produced in Qatar [27,28]. Most of the slag produced is dumped in landfills due to a lack of field utilization of such a product [29,30]. Landfilling of these vast quantities of slag harms the environment, as they contain heavy and toxic metals [27]. Therefore, utilizing SSA in concrete applications would not only save landfill spaces and preserve NA sources but also reduce toxic gases in the environment. Despite the toxic metals in SSA, previous studies demonstrated that using SSA in concrete applications is safe for human and animal health [31,32]. Several studies have investigated the mechanical properties of SSA concrete. Sohail et al. [27] and Roslan et al. [33] found that SSA concrete had considerably lower slump than NA concrete. Pellegrino and Gaddo [34] showed that the compressive strength of SSA concrete was 38% higher than that of NA concrete. A similar conclusion was also made by other researchers [34–40]. Qasrawi [35] noticed that the use of 100% SSA increased the flexural tensile strength of concrete by about 50%. Alnahhal et al. [28] and Awoyera et al. [36] also observed an increase in the flexural strength of concrete when NA were replaced by SSA. On the other hand, limited studies have been conducted on the durability properties of SSA concrete [41,42]. Tran et al. [41] and Ting et al. [43] demonstrated that HPC with SSA achieved better chloride resistance and resistivity than conventional HPC. Ortega-López et al. [44] found that the carbonation and permeability resistance were noticeably improved when SSA were used in concrete. Heniegal et al. [42] showed that concrete specimens incorporating SSA and silica fume (SF) had higher corrosion resistance than conventional concrete. Moreover, the conductivity of SSA concrete is considerably higher than NA concrete [45].

On the other hand, reinforced concrete degradation by chloride ions and carbonation is a problem of growing concern among researchers, especially in coastal areas. Sohail et al. [46] found that the carbonation and chloride of 30 to 40-year-old structures in Qatar were six times higher than the threshold values for corrosion initiation in mild steel. Employing RCA and SSA in concrete applications may further deteriorate concrete durability properties because of the contaminated products on RCA and SSA surface. Therefore, there is a need to replace NSC with a more durable product, like ultra-high performance concrete (UHPC) [46–50]. The UHPC has superior durability and mechanical properties compared to conventional NSC and HPC [51]. As per ASTM C1856/C1856M − 20 provisions [52], UHPC is defined as a cementitious material with a minimum of 120 MPa compressive strength and 200–250 mm flowability in accordance with ASTM C1437 [53], agreeing with almost all studies [46–51,54–56]. UHPC mixes are produced using a very low water-to-binder (W/B) ratio [57]. The workability of UHPC can be improved by replacing the un-hydrated cement with SF, fly ash (FA), and blast furnace slag [57]. Incorporating these additives also enhances the UHPC's particle packing density and improves the mechanical and durability properties of UHPC. Nevertheless, UHPC is a very brittle material in nature and might experience excessive cracks on its surface due to its high strength [51]. Therefore, discrete fibers should be added to UHPC mixes to absorb the tensile stresses and enhance the UHPC's ductility [51]. Several studies investigated the mechanical and durability properties of plain and ultra-high performance fiber reinforced concrete (UHPFRC). Sohail et al. [51] and Dobias et al. [58] found that UHPC specimens exhibited five times lower water absorption than NSC. Roux et al. [54] revealed that UHPC had 82% lower chloride diffusion than NSC. Likewise, Sohail et al. [51] showed that UHPC had 99% and 72% lower chloride permeability and sorptivity than NSC, respectively. Bonneau et al. [59] reported that steel fibers slightly increased the compressive strength of UHPC. Similarly, Abbas et al. [57] revealed that the compressive and flexural strengths of UHPC increased by 13% and 37%, respectively, by incorporating steel fibers. Kazemi and Lubell [60] achieved higher UHPC ductility by incorporating steel fibers. Abbas et al. [57] showed that incorporating higher dosages of steel fibers to UHPC mixes decreased the chloride permeability by 53%.

By far, limited studies have been performed on the characteristics of UHPC with RCA, SSA, and steel fibers. Yu et al. [49] utilized fine RCA in UHPC and found that at a 100% RCA replacement ratio, the compressive strength increased by 20%, while the flexural strength decreased by 40%, compared to conventional UHPC. Zhang et al. [61] showed that the compressive and flexural strengths of UHPC decreased as the fine RCA replacement ratio increased. In addition, Liu and Guo [62] prepared UHPC using SSA and observed that UHPC with SSA achieved higher compressive strength than conventional UHPC. Other recyclable materials such as ceramic waste, ultrafine palm oil fuel ash, plastic polyethylene terephthalate, and recycled coral were also used to produce UHPC [47,48,61,63,64].

As presented above, most of the previous studies have focused only on the influence of RCA and SSA on the mechanical and durability properties of NSC and HPC. Nonetheless, studies on the effect of RCA and SSA on UHPFRC have not been performed yet. This study was therefore needed to fill the gap in the literature. In this study, the effect of coarse RCA and SSA on the compressive strength, flexural strength, resistivity, porosity, and chloride permeability of UHPFRC was experimentally investigated using 144 specimens. It is anticipated that this study would contribute to minimizing C&D waste, reducing UHPC costs, and preserving natural resources.

2. Experimental program

The experimental program of the current study consisted of mechanical and durability testing of 144 UHPFRC specimens, including 108 cylinders (100 × 200 mm) and 36 prisms (100 × 100 × 500 mm). A flowchart describing the experimental program and its link to the results is shown in Fig. 1.

2.1. Materials

UHPC mixes' ingredients used in the current study were OPC, water, sand, coarse aggregates, steel fibers, superplasticizers (SP), and supplementary cementitious materials (SCM) (SF and class F FA). The chemical composition of all UHPC ingredients was determined by X-ray fluorescence (XRF) analysis and tabulated in Table 1.

2.1.1. Cementitious materials and sand

An ordinary Portland cement type CEM I 42.5 R, complying with ASTM C150/C150M − 20 requirements [65], was used in this study. The OPC used had a particle size range of 10–90 μm. Moreover, SF and FA with a particle size range of 0.1–10 and 3–55 μm, respectively, were used to enhance the pozzolanic reaction and flowability of UHPC. Sand was sieved into two sizes: sand-1 and sand-2 with a particle size range of

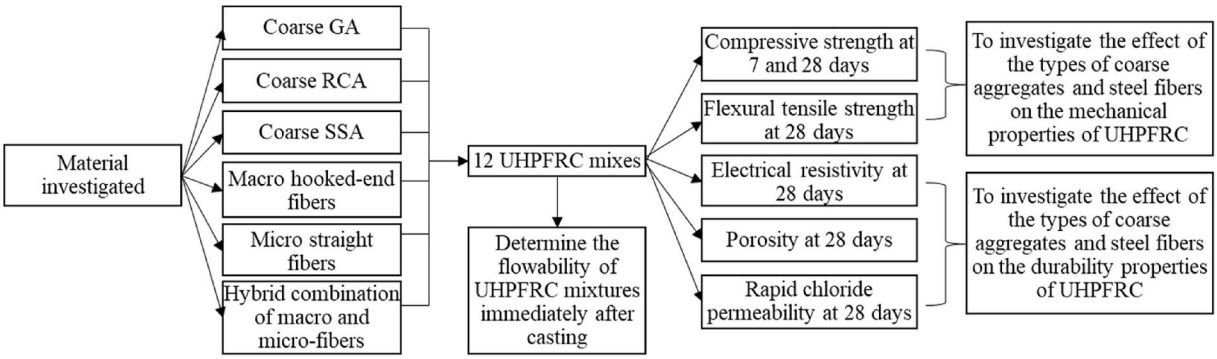

Fig. 1. Flowchart of the experimental program.

Table 1
Oxide compositions of OPC, SF, FA, sand-1, sand-2, GA, RCA, and SSA.

Oxide (%)	OPC	SF	FA	Sand-1	Sand-2	GA	RCA	SSA
Na_2O	–	0.04	0.06	–	–	2.3	1.1	0.8
MgO	2	0.23	1.57	0.9	0.91	6.7	12.5	5.8
Al_2O_3	3.18	1.44	28.49	3.9	4.11	15.1	1.7	3.7
SiO_2	15.74	94.5	55.97	67.05	75.09	44.9	53.9	18.8
P_2O_5	–	0.53	0.62	1.3	0.93	–	0.1	0.3
SO_3	3.8	2.14	0.51	4.78	2.31	0.1	0.8	0.1
CL	0.05	0.16	0.12	1.71	2.13	–	–	–
K_2O	0.47	0.37	1	0.7	0.02	–	0.2	–
CaO	68.91	0.13	2.74	17.44	12.71	–	–	0.1
TiO_2	0.28	–	1.95	0.23	0.16	–	–	1
V_2O_5	0.05	–	0.04	–	–	–	–	1
Cr_2O_3	0.05	–	0.04	0.12	0.13	–	0.2	0.1
MnO	0.09	0.02	0.09	0.05	0.04	0.1	0.2	1.3
Fe_2O_3	4.8	0.42	6.63	1.7	1.35	16.5	18.2	47
Nio	–	–	0.02	0.04	–	0.1	0.2	–
SrO	0.05	–	0.06	0.08	0.05	–	–	–
ZrO_2	–	–	0.07	–	–	–	–	0.1
CaO	–	–	–	–	–	13.8	10.5	19.7
Total	99.47	99.98	99.98	100	99.94	99.6	99.6	99.8

Note: Total is less than 100% because lighter oxides are not detected by the equipment.

300–600 μm and 600–1180 μm, respectively. All UHPFRC mixes were made with a constant superplasticizer (SP) content of 1.5% of OPC weight.

2.1.2. Coarse aggregates

Three types of coarse aggregates were used in this study: natural gabbro (GA), RCA, and SSA. Photographs of these aggregates are shown in Fig. 2(a)–(c). The coarse aggregate size was limited to 10 mm to minimize their effect on the macrostructure, flowability, and homogeneity of UHPC. The properties of the three aggregate types along with Qatar Construction Specifications (QCS-2014) limits [66] are listed in Table 2. As shown in the table, all properties were within the acceptable limits of QCS-2014 [66], except for the water absorption of RCA. The water absorption of RCA surpassed the maximum limit of QCS-2014 [66] by 103%. The results also indicate that SSA have higher specific gravity than GA and RCA. In addition, RCA and SSA have higher material loss than GA. Moreover, RCA have lower resistance to weathering than GA and SSA. The three types of aggregates were in the SSD condition before mixing to ensure uniformity in the aggregate water absorption and free voids. This was achieved by soaking the aggregates in water for 24 h before mixing, as recommended by Alnahhal and Aljidda [12], Sohail et al. [27], and Butler et al. [71].

2.1.3. Steel fibers

Three types of fiber reinforcement were employed: macro hooked-end fibers, micro straight fibers, and a hybrid combination of these two fibers. As shown in Fig. 3, steel macro-fibers are hooked at both ends and characterized by a low carbon coating, while steel micro-fibers are straight and have a brass coating. The length, diameter, and tensile strength of the steel fibers are presented in Table 3.

2.2. UHPFRC mix proportions

A total of 12 UHPFRC mixes were prepared with different coarse aggregate types (i.e., GA, RCA, and SSA) and steel fiber types (i.e., macro, micro, and hybrid combination of macro and micro-fibers). The coarse aggregates were limited to 12.5% of the total UHPFRCs' volume to minimize their effect on the UHPFRCs' macrostructure. Steel fibers were added at a volume fractions (V_f) of 1% for all UHPFRC mixes. Specimens with a hybrid combination of steel micro and macro-fibers with a volume fraction of 0.5% each were also investigated in this study. Table 4 presents the proportions of the 12 UHPFRC mixtures. Specimens' nomenclature was designated based on the coarse aggregate type (i.e., G, S, and R for GA, SSA, and RCA, respectively), followed by the steel fiber type (i.e., P refers to plain concrete, while MA, MI, and MA/MI refer to macro-fibers, micro-fibers, and a hybrid combination of steel macro and micro-fibers, respectively). For example, mix G-P refers to a UHPC mix made with GA and no fibers. Mix G-P was developed through trials by adjusting the OPC, SF, FA, and aggregate contents; then, GA were entirely replaced by weight with RCA and SSA in mixtures R–P and S–P, respectively; after that, steel macro and micro-fibers were added at a V_f of 1.0%, or a combination of 0.5% for each.

2.3. Mixing procedure

All UHPFRC mixes were prepared using a 95-l volume capacity pan mixer by adopting the following mixing procedure: first, dry ingredients (i.e., aggregates, cement, SF, FA, sand-1, and sand-2) were dry mixed for 5 min; next, water and half of the SP were gradually added to the dry mix and mixed for another 3 min; the remaining of SP was then added and continued mixing for another 3 min; finally, steel fibers were added, and the mixing resumed until a homogeneous mixture was obtained. After casting, UHPC was immediately placed in the molds in three layers and compacted using a vibrating table. After 24 h, specimens were demolded and cured in a water tank until the test day.

2.4. Mechanical and durability evaluation tests

2.4.1. Fresh and hardened mechanical properties

The fresh and hardened mechanical properties of UHPC, including the flowability, compressive strength, and flexural tensile strength, were carried out to evaluate the influence of different coarse aggregate and steel fiber types on the mechanical characteristics of UHPFRC. The details of the performed tests are provided in the following subsections:

2.4.1.1. Flowability. To measure the flowability of the UHPFRC mixes, a

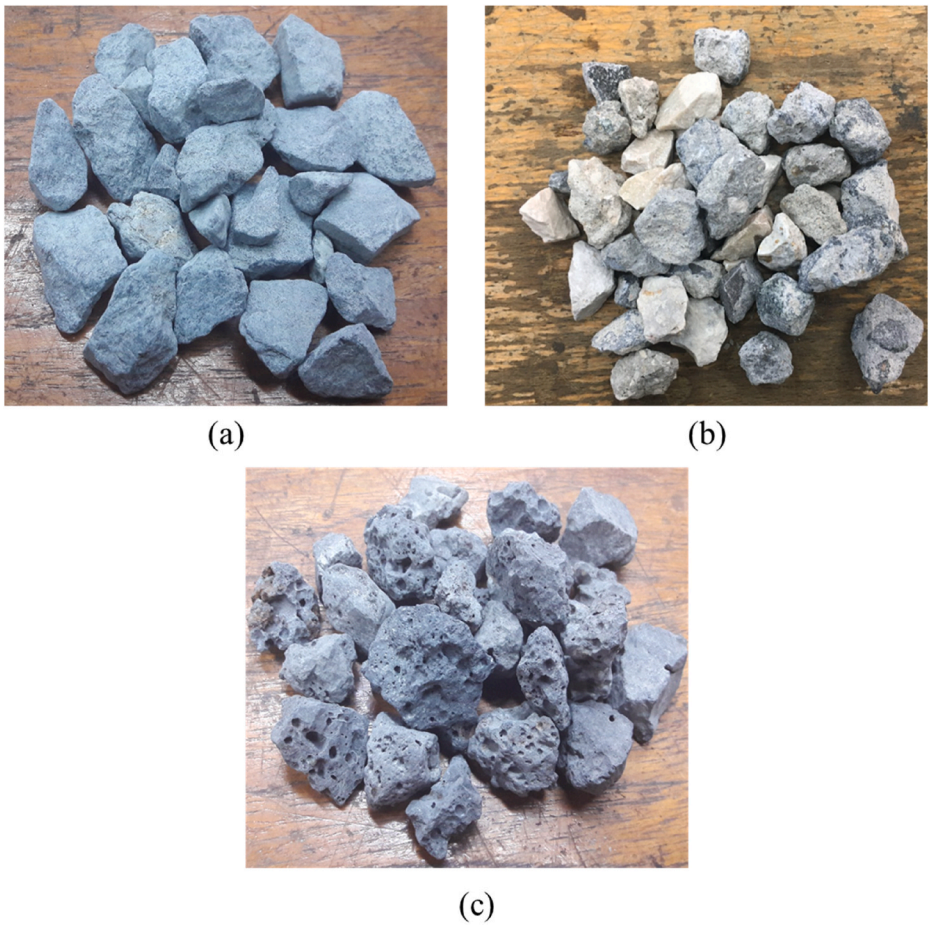

Fig. 2. Coarse aggregate used in this study: (a) GA, (b) RCA, and (c) SSA.

flow table test was immediately performed after casting as per ASTM C1611/C1611M − 21 [72] provisions. During the test, UHPFRC was first poured into an inverted slump cone; then, the cone was lifted upwards in about 5 s to allow UHPC to flow freely outwards; finally, the mean value of two perpendicular diameters was recorded and considered as the UHPFRC flowability.

2.4.1.2. Compressive strength. The compressive strength of UHPFRC was evaluated following ASTM C39/C39 M − 20 standards [73]. Six cylinders (100 × 200 mm) were prepared from each UHPC mix. The prepared specimens were kept in a curing tank for 7 and 28 days. At the testing date, the specimens were compressed at a loading rate of 0.25 MPa/s.

2.4.1.3. Flexural tensile strength. Flexural tensile strength tests were performed at 28 days as per ASTM C1609/C1609M − 12 provisions [74]. Three prisms (100 × 100 × 500 mm) were prepared from each UHPFRC mix and tested at a displacement rate of 0.1 mm/min.

2.4.2. Durability properties

To assess the durability of UHPFRC mixes, resistivity, porosity, and rapid chloride permeability tests were performed. The details of each test are described in the following subsections:

2.4.2.1. Electrical resistivity. Electrical resistivity tests were performed on three cylinders (100 × 200 mm) at 28 days using the four-point electrical Wenner probe Giatec® resistivity meter device as per AASHTO TP 95 standards [75]. The test measures how easily electric current can move through concrete specimens. Resistivity results are sensitive to humidity and degree of saturation [51]. Therefore, all specimens were tested in the SSD condition. Table 5 presents the corrosion risk as a function of the resistivity values. Corrosion risk is classified as a function of resistivity as high, moderate, low, very low, and negligible. Higher resistivity indicates dense microstructure and less corrosion risk and vice versa.

Table 2
Aggregate physical properties compared to (QCS-2014) [66] limits.

Property	Specification	GA	RCA	SSA	(QCS-2014) Limit [66]
Bulk Dry Specific Gravity (%)	ASTM C127–15 [67]	2.88	1.96	3.24	–
Bulk SSD Specific Gravity (%)	ASTM C127–15 [67]	2.89	2.04	3.31	–
Bulk Apparent Specific Gravity (%)	ASTM C127–15 [67]	2.93	2.13	3.48	–
Water Absorption (%)	ASTM C127–15 [67]	0.68	4.06	1.06	2
Elongation Index (%)	ASTM D4791–19 [68]	24.0	8.00	13.0	35
Los Angeles Abrasion (%)	ASTM C131–20 [69]	8.10	27.84	14.9	30
Soundness (%)	ASTM C88/C88M − 18 [70]	2.17	12.6	1.00	15

Fig. 3. Steel fiber used in this study: (a) macro hooked-end fibers and (b) micro straight fibers.

Table 3
Physical properties of the steel fibers.

Steel fiber type	Length (mm)	Diameter (mm)	Tensile strength (MPa)
Steel macro-fibers	50	0.9	1100
Steel micro-fibers	6	0.2	2750

2.4.2.2. Rapid chloride permeability test (RCPT). The RCPT was performed at 28 days on two cylinders (100 × 50 mm) sliced from a 100 × 200 mm cylinder in accordance with ASTM C1202-19 standards [76]. The RCPT measures in Coulomb charge how easily chloride ions can permeate concrete pores. The specimens were first dried in an oven at 50 °C for 3 days; the specimens' circumferences were then sealed by silicone epoxy and vacuumed inside a desiccator for 3 h; after that, the specimens were fully immersed in water and continued vacuuming for 18 h; eventually, the specimens were placed inside polyacrylic boxes and sealed. As specified in ASTM C1202-19 standards [76], the boxes were filled on one side with 0.3 N concentrated sodium hydroxide (NaOH) solution and on the other side with 3% concentrated sodium chloride (NaCl) solution. The tests continued for 6 h, and the applied current (Amperes) was recorded every 30 min. Coulomb charges transferred were calculated as per Eq. (1):

$$Q = 900(I_0 + 2I_{30} + 2I_{60} + \cdots + 2I_{300} + 2I_{330} + I_{360}) \quad (1)$$

where I_0, I_{30}, I_{60}, etc. are the applied current at the start, after 30 min, after 60 min, etc.

2.4.2.3. Porosity. To evaluate the influence of coarse aggregate and steel fiber types on the pores of UHPC, the porosity of UHPFRC was measured at 28 days on two cylinders (100 × 50 mm) as per ASTM C1754/C1754M – 12 provisions [77]. The specimens were sliced from a 100 × 200 mm cylinder. The sliced specimens were first dried in an oven at 38 °C for 24 h and weighed; then, the dried specimens were returned to the oven and reweighed every 24 h until a difference of 0.5% was achieved between two cycles; after that, the specimens were immersed in water for 30 min, and the submerged weight was recorded. The porosity was calculated as per Eq. (2):

$$\textit{Void content} = \left[1 - \left(\frac{K \times (A - B)}{\rho_w \times D^2 \times L}\right)\right] \times 100 \quad (2)$$

where K is a constant (1,273,240 $mm^3 kg/m^3 g$), A is the dry weight (g), B is the submerged weight (g), ρ_w is the water density (kg/m^3), D is the specimen's diameter, and L is the specimen's height.

Table 5
Corrosion risks as a function of the electrical resistivity (AASHTO TP 95 [75]).

Resistivity (kΩ•cm)	Corrosion Risk
<12	High
12 to 21	Moderate
21 to 37	Low
37 to 254	Very Low
>254	Negligible

Table 4
UHPFRC mix proportions.

Material	G-P	G-MA	G-MI	G-MA/MI	S–P	S-MA	S-MI	S-MA/MI	R–P	R-MA	R-MI	R-MA/MI
	kg/m^3											
Cement	770	770	770	770	770	770	770	770	770	770	770	770
Sand-1	154	154	154	154	154	154	154	154	154	154	154	154
Sand-2	308	308	308	308	308	308	308	308	308	308	308	308
FA	192.5	192.5	192.5	192.5	192.5	192.5	192.5	192.5	192.5	192.5	192.5	192.5
SF	192.5	192.5	192.5	192.5	192.5	192.5	192.5	192.5	192.5	192.5	192.5	192.5
Water	177	177	177	177	177	177	177	177	177	177	177	177
GA	226	226	226	226	0	0	0	0	0	0	0	0
SSA	0	0	0	0	226	226	226	226	0	0	0	0
RCA	0	0	0	0	0	0	0	0	226	226	226	226
Micro-fibers	0	0	18	9	0	0	18	9	0	0	18	9
Macro-fibers	0	18	0	9	0	18	0	9	0	18	0	9
SP	11.6	11.6	11.6	11.6	11.6	11.6	11.6	11.6	11.6	11.6	11.6	11.6

3. Results and discussion

3.1. Fresh and hardened mechanical properties

3.1.1. UHPFRC flowability

The flowability test results of all UHPFRC mixes are listed in Table 6. It could be seen that there was no significant difference in the UHPC flowability between the control mix and its counterparts with SSA and RCA. That was because the three types of aggregates were in the SSD condition, which ensured uniformity in aggregates' water absorption and free voids. A study conducted by Alnahhal and Aljidda [12] indicated that when NA and RCA were utilized in the SSD condition, NA and RCA concrete recorded approximately similar slump values. Besides, the UHPC flowability slightly decreased by 12%−15% with the addition of steel fibers, attributable to the friction between the steel fibers and the matrix. Abbas et al. [57] have also reported that steel fibers decreased the flowability of UHPC by approximately 13%.

3.1.2. Compressive strength

The 7 and 28-day compressive strengths of all UHPC mixes are shown in Fig. 4(a)–(d). The results showed that all UHPC mixes achieved the minimum compressive strength at 28 days (i.e., 120 MPa), specified in ASTM C1856/C1856M − 20 provisions [52]. In addition, the 28-day specimens of all UHPC mixes had an average of 19% higher compressive strength than the 7-day specimens, owing to the progressive cement hydration over time and secondary pozzolanic reactions between SCM (i.e., SF and FA) and $Ca(OH)_2$, which densified the UHPCs' microstructure [57,78]. Furthermore, the aggregate type showed little effect on the UHPC compressive strength at both curing periods (Fig. 4(a)). Replacing GA by SSA in mix S–P slightly increased the 7 and 28-day compressive strength by 8% and 3%, respectively. This increase could be linked to the high specific gravity and rough surface texture of SSA compared to GA, which improved the adhesive force between aggregates and cement mortar. On the contrary, replacing GA by RCA in mix R–P slightly decreased the 7 and 28-day compressive strength by 5.7% and 6.4%, respectively, owing to the presence of old mortar on the RCA, which created a secondary ITZ layer between old and new mortars and increased UHPCs' pores and water absorption [5]. The decrease in the compressive strength of mix R–P might also be linked to the low specific gravity of RCA in comparison with GA and SSA (see Table 2). Even though the compressive strength decreased with RCA, the decrease is still relatively low compared to Younis et al. [15] and Wagih et al. [16], who reported that RCA decreased the compressive strength by 15%–33%. That was because the coarse aggregates in the current study were accounted for only 12.5% of the total UHPCs' volume, and thus the effect of RCA on UHPCs' pores, density, and ITZ layers was minimized. The slight effect of RCA on UHPC compressive strength in this study could also be related to the SSD surface condition of both GA and RCA, of which having RCA in SSD condition ensures that all voids are filled with water. The obtained results are consistent with Alnahhal and Aljidda [12] and Alnahhal et al. [28] for RCA and SSA concretes, respectively.

Table 6
Flowability test results of UHPFRC mixes.

Mix	Flowability (mm)
G-P	750
G-MA	640
G-MI	660
G-MA/MI	650
S–P	725
S-MA	615
S-MI	635
S-MA/MI	620
R–P	740
R-MA	610
R-MI	630
R-MA/MI	640

Fig. 4(b)–(d) shows that the steel macro-fibers slightly affected the UHPCs' compressive strength, whereas steel micro-fibers and the hybrid use of steel macro and micro-fibers had a more noticeable effect on the UHPFRCs' compressive strength, irrespective of aggregate type. It is worth noting that the enhancement in the compressive strength with steel fibers was more pronounced for the 28-day specimens compared to those of the 7-day specimens. This might be attributed to the progressive cement hydration over time, which produced more cement hydration products, which, in turn, increased the bond strength between the matrix and fibers and consequently enhanced the bridging action of the fibers. The 28-day compressive strength of specimens G-MA and S-MA were almost similar to their counterpart plain specimens, and specimen R-MA had only 4.8% higher compressive strength than mix R–P. On the other hand, specimens S-MI, G-MI, R-MI, S-MA/MI, G-MA/MI, and R-MA/MI, recorded 10%, 2.5%, 8.9%, 10%, 7%, and 14.7% higher compressive strength at 28 days than their counterparts with no fibers, respectively. These observations could be attributed to the type of steel fiber used [79]. At the same V_f of steel fibers, the number of lower length-to-diameter ratio fibers (i.e., micro-fibers) available to absorb the developed stresses and bridge the initiated cracks is higher than that of higher length-to-diameter fibers (i.e., macro-fibers). Increasing the number of fibers in turn increases the adhesion with the cement matrix and ensures higher compressive strength. Furthermore, UHPFRC with micro-fibers has more densified microstructure and less entrapped air and fiber agglomeration than UHPFRC with macro-fibers, and hence UHPFRC with micro-fibers achieves higher compressive strength [79]. In conformance with these findings, Abbas et al. [57] showed that the compressive strength of UHPC increased with the addition of steel fibers. Moreover, Yoo et al. [80] revealed that hooked-end fibers have a poorer distribution in the matrix than straight fibers, and consequently the straight fibers were more efficient than the deformed fibers in enhancing the UHPFRC compressive strength.

3.1.3. Flexural tensile strength

As expected, it was observed that adding steel fibers to UHPFRCs' mixes restrained the opening and the propagation of the cracks and consequently changed the failure mode from brittle (Fig. 5(a)) to a more ductile failure (Fig. 5(b)). This improvement is ascribed to the crack bridging action of the fibers, which bridged the cacks and transferred the stresses through the whole length of the prism and thus enhanced the post-cracking response of the UHPFRC prisms. A similar response was also observed by other researchers with different types of concrete and fibers [57,81]. On the other hand, Fig. 6(a)–(d) depicts the measured 28-day flexural tensile strength of plain and UHPFRC prisms. Test results showed that specimen S–P had 9.8% higher flexural strength, while specimen R–P recorded 36.11% lower flexural strength than specimen G-P (Fig. 6(a)). The increase in the flexural strength with SSA was due to the angularity and rough surface texture of SSA, which create a dense ITZ layer and improve the adhesive force between aggregates and cement matrix [28]. However, UHPC with RCA showed lower flexural tensile strength because of the adhered mortar on RCA surface, which create an additional ITZ layer between old and new mortars and increase the UHPCs' pores and water absorption [20]. These findings are in agreement with Wang et al. [20], Sohail et al. [27], and Alnahhal et al. [28], who also observed that the flexural tensile strength of concrete was increased with SSA and decreased with RCA.

Furthermore, the flexural strength of UHPFRC was significantly improved with the addition of steel fibers (Fig. 6(b)–(d)). It is well documented that fibers maintain the integrity of concrete after the initiation of the first crack by redistributing the stresses along the cracks, and hence improves the ITZ layer between aggregates and cement matrix [79]. The gain in the UHPFRCs' flexural strength varied with the type of steel fibers used. UHPFRC prisms with macro hooked-end fibers, G-MA, S-MA, and R-MA, had 101.7%, 32.41%, and 169.24% higher flexural strength than their counterparts with no fibers, respectively. Nevertheless, UHPFRC prisms with straight micro-fibers recorded a

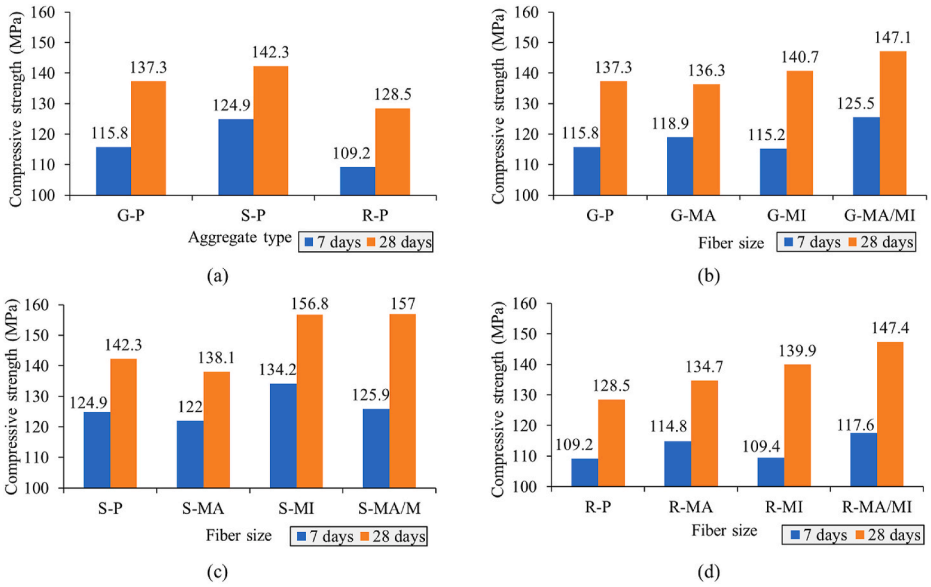

Fig. 4. Compressive strength test results: (a) plain specimens, (b) fiber-GA specimens, (c) fiber-SSA specimens, and (d) fiber-RCA specimens.

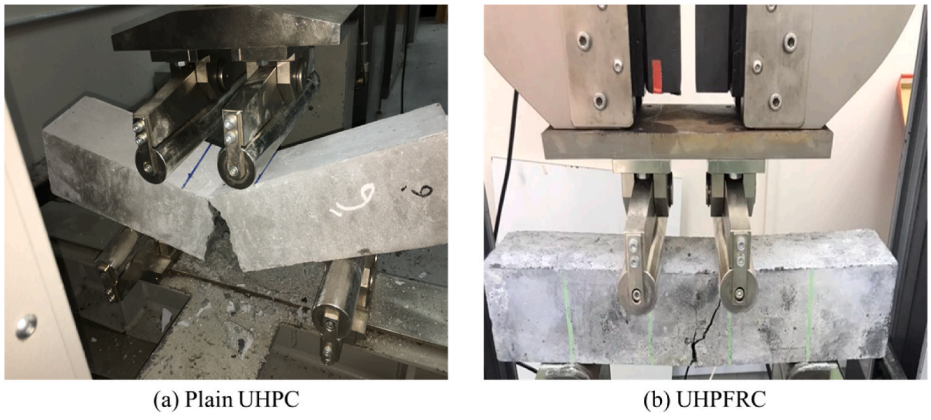

Fig. 5. Failure modes of UHPFRC in flexure.

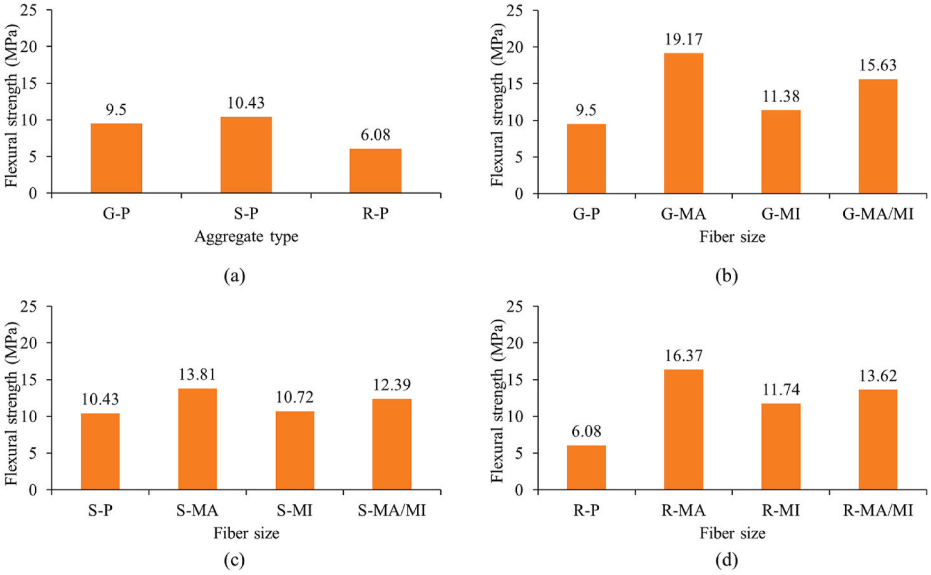

Fig. 6. Flexural strength test results: (a) plain specimens, (b) fiber-GA specimens, (c) fiber-SSA specimens, and (d) fiber-RCA specimens.

lower rate of increase than UHPFRC prisms with macro hooked-end fibers. For example, UHPC prisms G-MI, S-MI, R-MI, G-MA/MI, S-MA/MI, and R-MA/MI, were improved by 61.89%, 2.78%, 93.09, 64.52%, 18.79%, and 124% compared to their counterparts with no fibers, respectively. The variation of the UHPC flexural strength results is attributed to the pull-out strength of steel fibers. Macro hooked-end fibers have higher pull-out strength with concrete and are able to bridge the macro cracks more efficiently than straight micro-fibers, and hence UHPFRC with macro-fibers achieved higher flexural strength. Similarly, Kim et al. [82], Gesoglu et al. [83], Meng and Khayat [84], Zhang et al. [85], and Ma et al. [86] observed that UHPFRC with deformed fibers recorded noticeably higher flexural strength than UHPFRC with straight fibers.

It could also be recognized that the net gain in the flexural strength of UHPFRC prisms R-MA, R-MI, and R-MA/MI was higher than those with GA and SSA. Moreover, it could be seen that the flexural strength of prism R-MA outperformed that of prism S-MA, knowing that the performance of prism R–P was worse than that of S–P. This indicates that the addition of steel fibers to RCA concrete bridged the secondary ITZ layers between old and new mortars and consequently absorbed the tensile stresses at the weak ITZ layers. However, in the case of UHPFRC with SSA, the inclusion of the steel fibers had only maintained the UHPFRC's integrity and post-peak behavior. It could be concluded from these observations that the weak ITZ layer of RCA concrete could be enhanced by incorporating steel fibers.

3.1.4. Load-deflection behavior

Fig. 7(a)–(c) shows the load-deflection relationship of the UHPFRC tested specimens under flexural tensile strength tests. It is apparent from the figure that plain UHPFRC specimens experienced a sudden drop in the load-deflection response at failure, whilst UHPFRC specimens showed a more progressive failure and restrained residual loads after failure until the pull-out of steel fibers. It could also be noticed that UHPFRC prisms incorporating macro hook-end fibers exhibited higher stiffness (i.e., before reaching the peak load) than those with micro-fibers or a hybrid combination of both fiber types. Moreover, UHPFRC specimens with macro-fibers exhibited a steadier drop after the peak load rather than a steeper drop in the case of straight micro-fibers and hybrid combinations, indicating that more energy was released to pull or de-bond the macro hooked-end fibers from the matrix. This is fundamentally linked to the pull-out strength of steel fibers. As mentioned earlier, macro hooked-end fibers have higher pull-out strength with concrete and are able to bridge the macro cracks more efficiently than straight micro-fibers [79]. As a result, more energy was produced to pull-out or de-bond the hooked-end fiber from the matrix, and hence delayed the failure of UHPFRC prisms.

On the other hand, UHPFRCs' flexural properties, including cracking load and deflection, peak load and deflection, and toughness, were calculated according to the standardized equations of ASTM C1609/C1609M − 12 provisions [74] and listed in Table 7. UHPFRC specimens with hooked-end fibers exhibited better load and deflection responses at cracking and failure stages than those made with straight micro-fibers and hybrid combinations. For instance, specimen R-MA achieved 39.45% and 66.18% higher cracking load and 39.44% and 68.24% higher peak load than specimens R-MI and R-MA/MI, respectively. As well, specimen R-MA recorded 6.19% and 32.09% lower cracking deflection than specimens R-MI and R-MA/MI, respectively. Moreover, specimen R-MA reported higher peak deflection than its counterparts with straight micro-fibers and a hybrid combination of both fiber types, indicating that specimen R-MA had higher ductility than R-MI and R-MA/MI. Likewise, test results showed that UHPFRC specimens with macro hooked-end fibers reported higher toughness than UHPFRC specimens with straight micro-fibers or hybrid combinations. That was because more energy was consumed to pull or de-bond macro hooked-end fibers from the matrix compared to straight micro-fibers. These observations are in line with the findings of Abbas et al. [57].

3.2. Durability properties

3.2.1. Electrical resistivity

The 28-day electrical resistivity results of the plain and UHPFRC specimens are presented in Fig. 8(a)–(d). It could be observed that the

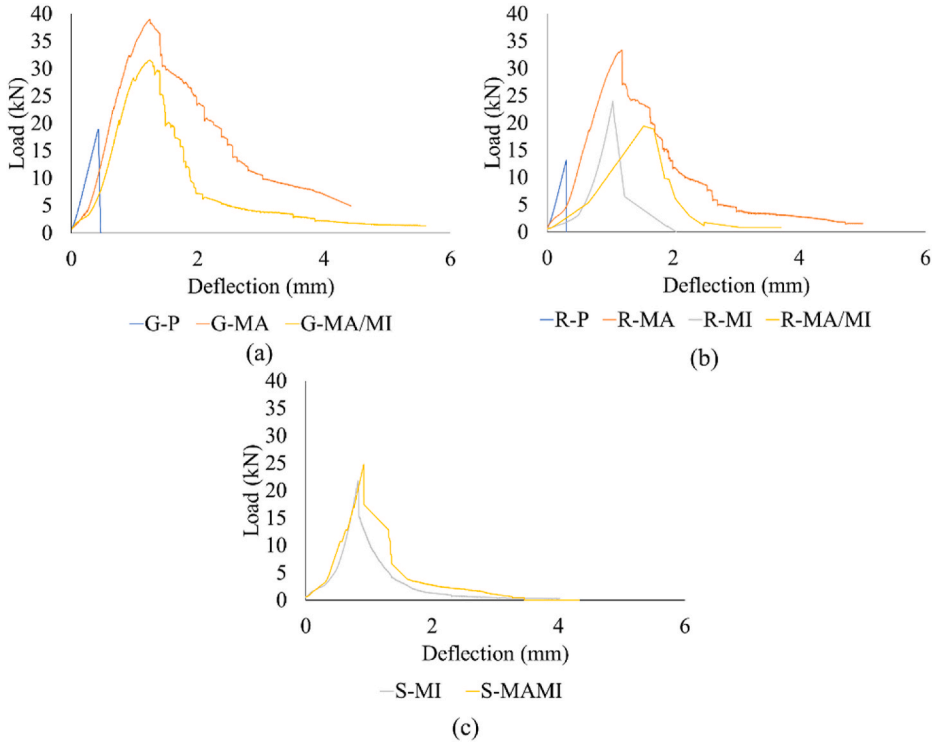

Fig. 7. Load-deflection curves for UHPFRC beam specimens with: (a) GA, (b) RCA, and (c) SSA.

Table 7
Flexural properties of UHPFRC prisms.

Prism	Cracking load (kN)	Cracking deflection (mm)	Peak load (kN)	Peak deflection (mm)	Toughness (kN•mm)
G-P	18.64	0.43	18.64	0.43	04.42
G-MA	32.10	0.94	38.33	1.22	63.82
G-MA/MI	27.91	0.99	31.26	1.25	46.89
R–P	12.16	0.31	12.16	0.31	01.95
R-MA	27.32	0.91	32.74	1.18	54.02
R-MI	19.59	0.97	23.48	1.04	17.95
R-MA/MI	16.44	1.34	19.46	1.16	12.65
S-MI	15.22	0.72	21.43	0.83	21.43
S-MA/MI	16.94	0.77	24.78	0.91	30.98

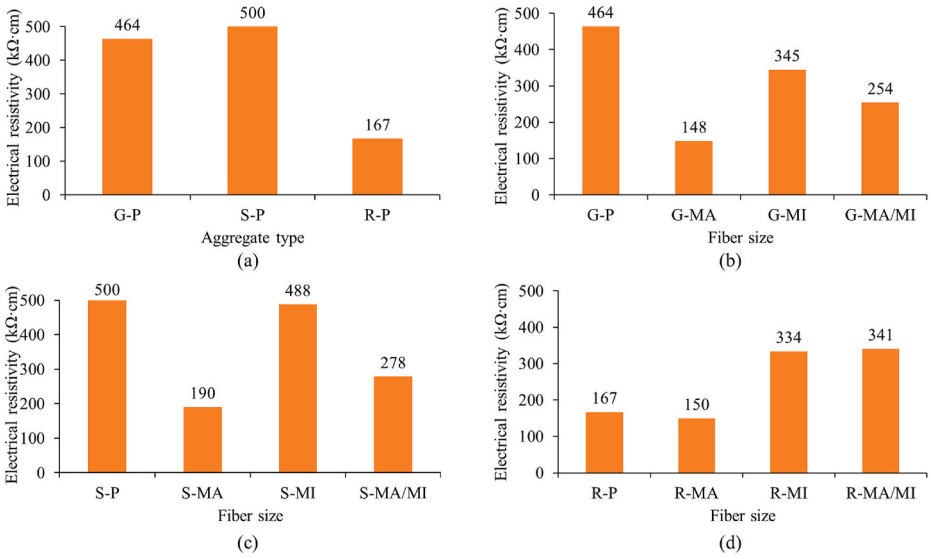

Fig. 8. Electrical resistivity test results: (a) plain specimens, (b) fiber-GA specimens, (c) fiber-SSA specimens, and (d) fiber-RCA specimens.

corrosion risk of all UHPFRC mixtures falls under two categories: "very low" and "negligible", as per AASHTO TP 95 standards [75]. Fig. 8(a) shows that the electrical resistivity was significantly affected by the aggregate type. Replacing GA by SSA in mix S–P increased the electrical resistivity by 7.7% due to the angularity and rough surface texture of SSA, which increased the interlocking and adhesive force between aggregates and cement matrix. Conversely, replacing GA by RCA in mix R–P decreased the electrical resistivity by 64% even though RCA were in SSD condition. That was because filling RCAs' pores with water promotes the movement of electrical charges, as water is a conductive element. Similar results were also obtained by Heniegal et al. [42] for SSA concrete and Andreu and Mire [25] and Kurda et al. [87] for RCA concrete.

Similar to the flexural strength results, Fig. 8(b)–(d) illustrates that the steel fibers have significantly affected the electrical resistivity of UHPFRC specimens. Compared to specimen G-P, the electrical resistivity of specimens G-MA, G-MI, and G-MA/MI were decreased by 68%, 26%, and 45%, respectively. This could be linked to the steel fibers' conductivity, which accelerated the movement of the electrical current through the UHPFRC. UHPFRC specimens with SSA had a similar trend to that of GA specimens. The drop in UHPFRCs' resistivity with steel macro-fibers could also be attributed to the poorer fiber distribution in the matrix, which resulted in more pores [79]. On the other hand, specimens R-MI and R-MA/MI exceeded their counterpart plain specimen by 100% and 104%, respectively. This enhancement indicates that the ITZ layer between cement matrix and aggregates was enhanced and thus decreased the micropores in the matrix. Similar results were also reported by Abbas et al. [57] and Banthia and Bhargava [88].

3.2.2. Porosity

The variations of the UHPFRC porosity at 28 days with different coarse aggregate and steel fiber types are presented in Fig. 9(a)–(d). The results revealed that the porosity of all UHPFRC specimens ranged from 0.86% to 3.41%, which is about 30% lower than that of NSC specimens [51]. The low porosity of UHPC is attributed to the fine sand, FA, and SF particles and their pozzolanic reaction product calcium-silicate hydrates (C–S–H), which fill the free voids, densify the microstructure of the UHPC, and improve the ITZ layers [57]. Similar to the electrical resistivity results, specimen S–P had 61% lower porosity than G-P, owing to the rough surface texture and angularity of SSA, which improved the adhesive force between aggregates and cement matrix and thus decreased UHPCs' pores (Fig. 9(a)). In contrast to electrical resistivity results, specimen R–P showed approximately similar porosity to that of G-P. This is probably linked to the SSD surface condition of GA and RCA, which ensured that all free voids in RCA were filled with water and consequently achieved uniformity in the aggregate water absorption and free voids. Likewise, Yu et al. [49] noticed that the porosity of UHPC was slightly influenced by fine RCA.

On the other hand, Fig. 9(b)–(d) shows that the trend of UHPFRCs' porosity was similar to that of compressive strength and electrical resistivity results. For example, mixes G-MA, S-MA, and R-MA had 47%, 33%, and 1% higher porosity than G-P, S–P, and R–P, respectively. This increase is ascribed to the poorer macro-fiber distribution in the matrix, which resulted in more macropores [79]. It could also be observed that the rate of deterioration of porosity in specimen R-MA was much lower than other UHPFRC specimens. This indicates an enhancement in the secondary ITZ layer between old and new mortars by the steel macro-fibers. Furthermore, adding steel micro-fibers to UHPFRC mixes noticeably improved the porosity of GA and RCA mixes by 16%–34%.

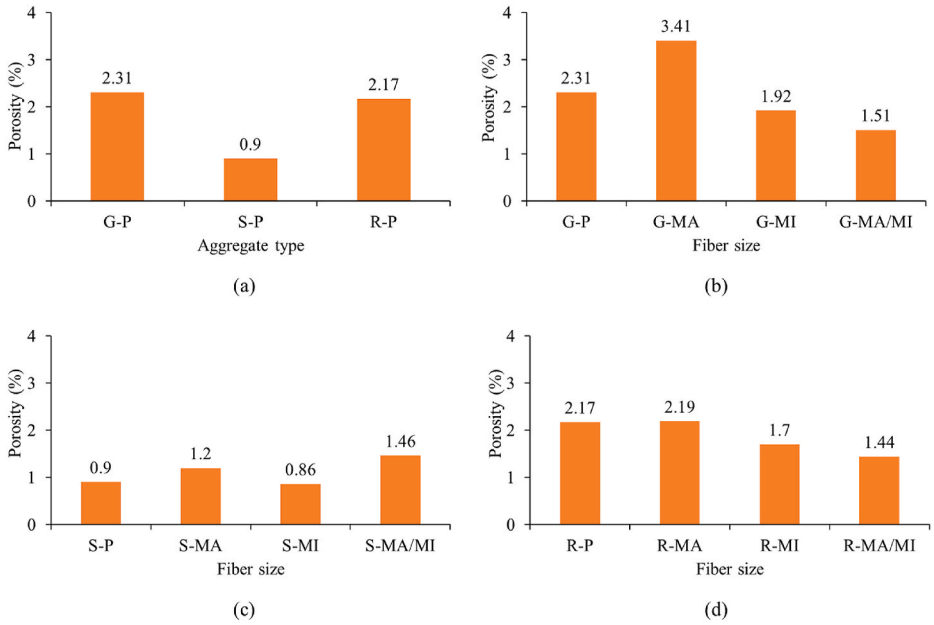

Fig. 9. Porosity test results: (a) plain specimens, (b) fiber-GA specimens, (c) fiber-SSA specimens, and (d) fiber-RCA specimens.

That was because UHPFRC specimens with steel micro-fibers have more densified microstructure and less entrapped air and fiber agglomeration than specimens with steel macro-fiber [79]. This indicates that UHPFRCs' porosity is highly correlated with the compressive strength and electrical resistivity results. These results agree with Toutanji et al. [89], who noticed that the permeability of UHPC increased with longer fibers and decreased with shorter fibers.

3.2.3. *Rapid chloride permeability*

The RCPT results for all UHPFRC mixes at 28 days are presented in Fig. 10(a)–(d). It could be observed that due to the dense microstructure of UHPC, RCPT results for all UHPC mixes ranged from 17 to 151 Coulombs, indicating "negligible" and "very low" chloride ion permeability as per ASTM C1202-19 standards [76]. Similar to electrical resistivity and porosity results, Fig. 10(a) shows that replacing GA by SSA in mix S–P decreased the Coulomb charges by 54.2% due to the rough surface texture and angularity of SSA, which improved the adhesive between aggregates and UHPC matrix. Conversely, mix R–P experienced a 76.4% increase in Coulomb charges compared to G-P. This is fundamentally attributed to the presence of old mortar on RCA, which created an additional ITZ layer between old and new mortars and hence increased the UHPC's pores and water absorption, even with filling RCAs' pores with water. That was because filling RCAs' pores with water promotes the movement of electrical charges, as water is a conductive element, as explained earlier in section 3.2.1. Similar results were also obtained by Rao et al. [90] and Saxena and Tembhurkar [37].

Moreover, the results illustrated that the steel fibers have a significant impact on Coulomb charges. In agreement with the compressive

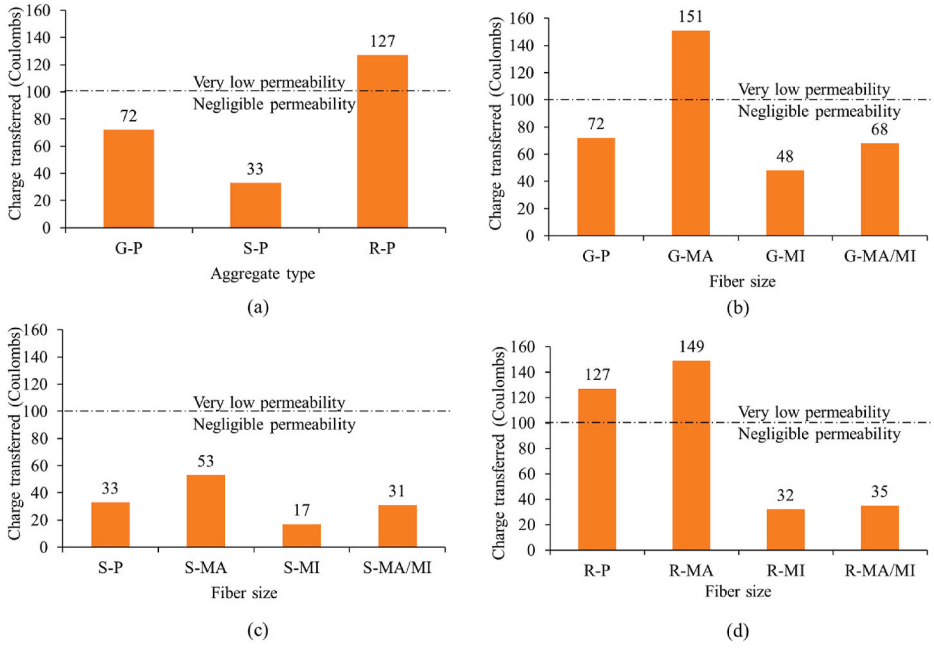

Fig. 10. RCPT test results: (a) plain specimens, (b) fiber-GA specimens, (c) fiber-SSA specimens, and (d) fiber-RCA specimens.

strength and porosity results, Fig. 10(b)–(d) shows that adding steel macro-fibers in mixes G-MA, S-MA, and R-MA increased the total charges by 109.7%, 60.6%, and 17.32%, respectively, compared to their counterparts with no fibers. This is attributed to the poorer macro-fiber distribution in the matrix, which resulted in more macropores [79]. However, the Coulomb charges decreased by incorporating steel micro-fibers. For example, UHPFRC specimens G-MI, S-MI, and R-MI reported 33.3%, 48.5%, and 74.8% lower charges than their counterparts with no fibers. As explained earlier, steel micro-fibers have better fiber distribution in the matrix than macro-fibers, and thus specimens G-MI, S-MI, and R-MI achieved a more densified microstructure than G-MA, S-MA, and R-MA. Likewise, the hybrid use of steel macro and micro-fibers in mixes G-MA/MI, G-MA/MI, and G-MA/MI resulted in 5.5%, 6%, and 72.4% lower Coulomb charges than their counterparts with no fibers, respectively. Similar to porosity results, the rate of improvement in specimen R-MI was higher than other specimens, indicating a noticeable in the secondary ITZ layer with steel micro-fibers. A study performed by Abbas et al. [57] confirmed that the use of shorter fibers densified the microstructure of the UHPFRC and consequently decreased the Coulomb charge transferred.

4. Conclusions

The feasibility of replacing natural GA by RCA and SSA in UHPFRC was investigated in this study. The assessment was carried out on the UHPFRC compressive and tensile strengths, electrical resistivity, porosity, and chloride permeability. The main conclusions of this study are as follows:

1. Replacing GA by RCA and SSA showed little effect on the compressive strength of UHPC. Furthermore, plain UHPC specimens and UHPFRC specimens with steel macro-fibers reported almost similar compressive strength. However, specimens incorporating steel micro-fibers and a hybrid combination of steel macro and micro-fibers recorded 2.5%–14.7% higher compressive strength than their counterparts with no fibers.
2. Replacing GA by RCA decreased the flexural tensile strength by 36.11%, whilst replacing GA by SSA increased the flexural strength by 9.8%.
3. UHPFRC prisms showed a progressive and more ductile failure mode than plain UHPC prisms. Moreover, a notable increase in the flexural tensile strength was observed when steel fibers were added. Prisms with macro-fibers showed 32.41%–169.24% higher flexural strength than plain UHPC prisms, while prisms with micro-fibers and hybrid combination of steel macro and micro-fibers recorded 2.78%–124% higher flexural strength than plain UHPC prisms.
4. Replacing GA by RCA significantly decreased the electrical resistivity by 64%. However, the incorporation of steel micro-fibers and hybrid combination of steel macro and micro-fibers increased the electrical resistivity by 104%. This indicates that the secondary ITZ layer between old and new mortars was enhanced with steel micro-fibers. Further studies are needed to confirm this conclusion.
5. UHPFRC porosity ranged between 0.86% and 3.41%, which is approximately 30% lower than NSC. Furthermore, replacing GA by SSA decreased the porosity by 61%, while replacing GA by RCA showed no significant difference. In addition, similar to electrical resistivity results, incorporating steel micro-fibers and hybrid combination of steel macro and micro-fibers in UHPFRC-RCA specimens decreased the porosity by 16%–34%.
6. Similar to electrical resistivity results, the Coulomb charges of specimen S–P decreased by 54.2%, whereas the charges increased by 76.4% in specimen R–P. Additionally, incorporating steel macro-fibers increased the Coulomb charges by 17.32%–109.7%. However, steel micro-fibers decreased the Coulomb charges by 33.3%–74.8% compared to plain UHPC specimens.

CRediT authorship contribution statement

Abdelrahman Abushanab: Investigation, Formal analysis, Data curation, Software, Writing – original draft, Visualization. **Wael Alnahhal:** Conceptualization, Methodology, Validation, Writing – review & editing, Resources, Funding acquisition, Supervision, Project administration. **Muazzam Ghous Sohail:** Investigation, Writing – review & editing. **Nasser Alnuaimi:** Funding acquisition, Supervision, Project administration. **Ramazan Kahraman:** Funding acquisition, Supervision, Project administration. **Nezam Altayeh:** Investigation, Formal analysis.

Declaration of competing interest

The authors declare that they have no known competing financial interests or personal relationships that could have appeared to influence the work reported in this paper.

Acknowledgment

This publication was made possible by GSRA grant GSRA6-1-0509-19022 from the Qatar National Research Fund (QNRF, a member of Qatar Foundation). Also, the authors show their gratitude to Qatar University for their financial support through the internal grant no. QUCG-CENG-20/21–3. Open Access funding provided by the Qatar National Library. The findings achieved herein are solely the responsibility of the authors.

References

[1] E. Aprianti S, A huge number of artificial waste material can be supplementary cementitious material (SCM) for concrete production – a review part II, J. Clean. Prod. 142 (2017) 4178–4194, https://doi.org/10.1016/j.jclepro.2015.12.115.
[2] C. Lima, A. Caggiano, C. Faella, E. Martinelli, M. Pepe, R. Realfonzo, Physical properties and mechanical behaviour of concrete made with recycled aggregates and fly ash, Construct. Build. Mater. 47 (2013) 547–559, https://doi.org/10.1016/j.conbuildmat.2013.04.051.
[3] S. Ahmed, Y. Alhoubi, N. Elmesalami, S. Yehia, F. Abed, Effect of recycled aggregates and treated wastewater on concrete subjected to different exposure conditions, Construct. Build. Mater. 266 (2021) 120930, https://doi.org/10.1016/j.conbuildmat.2020.120930.
[4] A. Akhtar, A.K. Sarmah, Construction and demolition waste generation and properties of recycled aggregate concrete: a global perspective, J. Clean. Prod. 186 (2018) 262–281, https://doi.org/10.1016/j.jclepro.2018.03.085.
[5] M. Al-Ansary, S.R. Iyengar, Physiochemical characterization of coarse aggregates in Qatar for construction industry, Int. J. Sustain. Built Environ. 2 (2013) 27–40, https://doi.org/10.1016/j.ijsbe.2013.07.003.
[6] D. Talamona, K. Hai Tan, Properties of recycled aggregate concrete for sustainable urban built environment, J. Sustain. Cem. Mater. 1 (2012) 202–210, https://doi.org/10.1080/21650373.2012.754571.
[7] C. Shi, Y. Li, J. Zhang, W. Li, L. Chong, Z. Xie, Performance enhancement of recycled concrete aggregate – a review, J. Clean. Prod. 112 (2016) 466–472, https://doi.org/10.1016/j.jclepro.2015.08.057.
[8] A. Coelho, J. de Brito, Economic viability analysis of a construction and demolition waste recycling plant in Portugal – part I: location, materials, technology and economic analysis, J. Clean. Prod. 39 (2013) 338–352, https://doi.org/10.1016/j.jclepro.2012.08.024.
[9] R. Jin, Q. Chen, Investigation of concrete recycling in the U.S. Construction industry, Procedia Eng 118 (2015) 894–901, https://doi.org/10.1016/j.proeng.2015.08.528.
[10] S.B. Huda, M.S. Alam, Mechanical and freeze-thaw durability properties of recycled aggregate concrete made with recycled coarse aggregate, J. Mater. Civ. Eng. 27 (2015) 4015003, https://doi.org/10.1061/(ASCE)MT.1943-5533.0001237.
[11] R. Kurda, J. de Brito, J.D. Silvestre, Influence of recycled aggregates and high contents of fly ash on concrete fresh properties, Cement Concr. Compos. 84 (2017) 198–213, https://doi.org/10.1016/j.cemconcomp.2017.09.009.
[12] W. Alnahhal, O. Aljidda, Flexural behavior of basalt fiber reinforced concrete beams with recycled concrete coarse aggregates, Construct. Build. Mater. 169 (2018) 165–178, https://doi.org/10.1016/j.conbuildmat.2018.02.135.
[13] B.M. Vinay Kumar, H. Ananthan, K.V.A. Balaji, Experimental studies on utilization of coarse and finer fractions of recycled concrete aggregates in self compacting concrete mixes, J. Build. Eng. 9 (2017) 100–108, https://doi.org/10.1016/j.jobe.2016.11.013.
[14] G. Dimitriou, P. Savva, M.F. Petrou, Enhancing mechanical and durability properties of recycled aggregate concrete, Construct. Build. Mater. 158 (2018) 228–235, https://doi.org/10.1016/j.conbuildmat.2017.09.137.

[15] A. Younis, U. Ebead, P. Suraneni, A. Nanni, Performance of seawater-mixed recycled-aggregate concrete, J. Mater. Civ. Eng. 32 (2020) 4019331, https://doi.org/10.1061/(ASCE)MT.1943-5533.0002999.
[16] A.M. Wagih, H.Z. El-Karmoty, M. Ebid, S.H. Okba, Recycled construction and demolition concrete waste as aggregate for structural concrete, HBRC J 9 (2013) 193–200, https://doi.org/10.1016/j.hbrcj.2013.08.007.
[17] C.S. Poon, S.C. Kou, L. Lam, Use of recycled aggregates in molded concrete bricks and blocks, Construct. Build. Mater. 16 (2002) 281–289, https://doi.org/10.1016/S0950-0618(02)00019-3.
[18] W. Alnahhal, Behaviour of fibre reinforced concrete using steel slag coarse aggregate produced in Qatar. MATEC Web Conf., 2017, https://doi.org/10.1051/matecconf/201712004004.
[19] A. Al-Hamrani, M. Kucukvar, W. Alnahhal, N. Mahdi, Green Concrete for a Circular Economy: A Review on Sustainability, Durability, and Structural Properties, Materials 14 (351) (2021), https://doi.org/10.3390/ma14020351.
[20] Y. Wang, P. Hughes, H. Niu, Y. Fan, A new method to improve the properties of recycled aggregate concrete: composite addition of basalt fiber and nano-silica, J. Clean. Prod. 236 (2019) 117602, https://doi.org/10.1016/j.jclepro.2019.07.077.
[21] J. Thomas, N.N. Thaickavil, P.M. Wilson, Strength and durability of concrete containing recycled concrete aggregates, J. Build. Eng. 19 (2018) 349–365, https://doi.org/10.1016/j.jobe.2018.05.007.
[22] S.K. Verma, D.K. Ashish, Mechanical behavior of concrete comprising successively recycled concrete aggregates, Adv. Concr. Constr. 5 (2017) 303, https://doi.org/10.12989/ACC.2017.5.4.303.
[23] J. de Brito, J. Ferreira, J. Pacheco, D. Soares, M. Guerreiro, Structural, material, mechanical and durability properties and behaviour of recycled aggregates concrete, J. Build. Eng. 6 (2016) 1–16, https://doi.org/10.1016/j.jobe.2016.02.003.
[24] B. Ali, L.A. Qureshi, S.H.A. Shah, S.U. Rehman, I. Hussain, M. Iqbal, A step towards durable, ductile and sustainable concrete: simultaneous incorporation of recycled aggregates, glass fiber and fly ash, Construct. Build. Mater. 251 (2020) 118980, https://doi.org/10.1016/j.conbuildmat.2020.118980.
[25] G. Andreu, E. Miren, Experimental analysis of properties of high performance recycled aggregate concrete, Construct. Build. Mater. 52 (2014) 227–235, https://doi.org/10.1016/j.conbuildmat.2013.11.054.
[26] C. Thomas, J. Setién, J.A. Polanco, Structural recycled aggregate concrete made with precast wastes, Construct. Build. Mater. 114 (2016) 536–546, https://doi.org/10.1016/j.conbuildmat.2016.03.203.
[27] M.G. Sohail, W. Alnahhal, A. Taha, K. Abdelaal, Sustainable alternative aggregates: characterization and influence on mechanical behavior of basalt fiber reinforced concrete, Construct. Build. Mater. 255 (2020) 119365, https://doi.org/10.1016/j.conbuildmat.2020.119365.
[28] W. Alnahhal, R. Taha, N. Alnuaimi, A. Al-Hamrani, Properties of fibre reinforced concrete made with discarded materials, Mag. Concr. Res. 71 (2018) 1–38, https://doi.org/10.1680/jmacr.17.00293.
[29] H. Yi, G. Xu, H. Cheng, J. Wang, Y. Wan, H. Chen, An overview of utilization of steel slag, Procedia Environ. Sci. 16 (2012) 791–801, https://doi.org/10.1016/j.proenv.2012.10.108.
[30] R. Taha, N. Al-Nuaimi, A. Kilayli, A. Ben Salem, Use of local discarded materials in concrete, Int. J. Sustain. Built Environ. 3 (2014) 35–46, https://doi.org/10.1016/j.ijsbe.2014.04.005.
[31] R.J. Collins, S.K. Ciesielski, Recycling and Use of Waste Materials and By-Products in Highway Construction, 1994.
[32] N.S. Association, Iron and steel making slag environmentally responsible construction aggregates, NSA Tech. Bull. (2003).
[33] N.H. Roslan, M. Ismail, Z. Abdul-Majid, S. Ghoreishiamiri, B. Muhammad, Performance of steel slag and steel sludge in concrete, Construct. Build. Mater. 104 (2016) 16–24, https://doi.org/10.1016/j.conbuildmat.2015.12.008.
[34] C. Pellegrino, V. Gaddo, Mechanical and durability characteristics of concrete containing EAF slag as aggregate, Cement Concr. Compos. 31 (2009) 663–671, https://doi.org/10.1016/j.cemconcomp.2009.05.006.
[35] H. Qasrawi, The use of steel slag aggregate to enhance the mechanical properties of recycled aggregate concrete and retain the environment, Construct. Build. Mater. 54 (2014) 298–304, https://doi.org/10.1016/j.conbuildmat.2013.12.063.
[36] P. Awoyera, O. Olofinnade, A. Busari, I. Akinwumi, M. Oyefesobi, M. Ikemefuna, Performance of steel slag aggregate concrete with varied water- cement ratio, J. Teknol. 78 (2016), https://doi.org/10.11113/jt.v78.8819.
[37] S. Saxena, A.R. Tembhurkar, Impact of use of steel slag as coarse aggregate and wastewater on fresh and hardened properties of concrete, Construct. Build. Mater. 165 (2018) 126–137, https://doi.org/10.1016/j.conbuildmat.2018.01.030.
[38] J.-Y. Lee, J.-M. Lee, C.-J. Wang, S.-W. Kim, H.-G. Kim, K.-H. Kim, Compressive stress distribution of concrete with EAF oxidising slag aggregates, Mag. Concr. Res. 70 (2017) 1–14, https://doi.org/10.1680/jmacr.16.00440.
[39] V. Maruthachalam, M. Palanisamy, High performance concrete with steel slag aggregate, Gradjevinar 66 (2014) 605–612, https://doi.org/10.14526/JCE.1052.2014.
[40] M.A. Khafaga, W.S. Fahmy, M.A. Sherif, A.M.N. Abdel Hamid, Properties of high strength concrete containing electric arc furnace steel slag aggregate, J. Eng. Sci. 42 (2014) 582–608.
[41] M. Tran, T. Nawa, B. Stitmannaithum, N. Chanh, Properties OF high strength concrete using steel slag coarse aggregate, Asean Eng. J. 4 (2015).
[42] A.M. Heniegal, M. Amin, H. Youssef, Effect of silica fume and steel slag coarse aggregate on the corrosion resistance of steel bars, Construct. Build. Mater. 155 (2017) 846–851, https://doi.org/10.1016/j.conbuildmat.2017.08.111.
[43] M.Z.Y. Ting, K.S. Wong, M.E. Rahman, M. Selowara Joo, Mechanical and durability performance of marine sand and seawater concrete incorporating silicomanganese slag as coarse aggregate, Construct. Build. Mater. 254 (2020) 119195.
[44] V. Ortega-López, J.A. Fuente-Alonso, A. Santamaría, J.T. San-José, Á. Aragón, Durability studies on fiber-reinforced EAF slag concrete for pavements, Construct. Build. Mater. 163 (2018) 471–481, https://doi.org/10.1016/j.conbuildmat.2017.12.121.
[45] Q. Dong, G. Wang, X. Chen, J. Tan, X. Gu, Recycling of steel slag aggregate in portland cement concrete: an overview, J. Clean. Prod. 282 (2021) 124447, https://doi.org/10.1016/j.jclepro.2020.124447.
[46] M.G. Sohail, R. Kahraman, N.G. Ozerkan, N.A. Alnuaimi, B. Gencturk, M. Dawood, A. Belarbi, Reinforced concrete degradation in the harsh climates of the arabian Gulf: field study on 30-to-50-Year-Old structures, J. Perform. Constr. Facil. 32 (2018) 4018059, https://doi.org/10.1061/(ASCE)CF.1943-5509.0001204.
[47] B. Zegardło, M. Szeląg, P. Ogrodnik, Ultra-high strength concrete made with recycled aggregate from sanitary ceramic wastes – the method of production and the interfacial transition zone, Construct. Build. Mater. 122 (2016) 736–742, https://doi.org/10.1016/j.conbuildmat.2016.06.112.
[48] A.H. Alani, N.M. Bunnori, A.T. Noaman, T.A. Majid, Durability performance of a novel ultra-high-performance PET green concrete (UHPPGC), Construct. Build. Mater. 209 (2019) 395–405, https://doi.org/10.1016/j.conbuildmat.2019.03.088.
[49] L. Yu, L. Huang, H. Ding, Rheological and mechanical properties of ultra-high-performance concrete containing fine recycled concrete aggregates, Materials 12 (2019) 3717, https://doi.org/10.3390/ma12223717.
[50] C.M. Tam, V.W.Y. Tam, K.M. Ng, Assessing drying shrinkage and water permeability of reactive powder concrete produced in Hong Kong, Construct. Build. Mater. 26 (2012) 79–89, https://doi.org/10.1016/j.conbuildmat.2011.05.006.
[51] M.G. Sohail, R. Kahraman, N. Al Nuaimi, B. Gencturk, W. Alnahhal, Durability characteristics of high and ultra-high performance concretes, J. Build. Eng. 33 (2021) 101669, https://doi.org/10.1016/j.jobe.2020.101669.
[52] ASTM C1856/C1856M − 20, Standard Practice for Fabricating and Testing Specimens of Ultra-High Performance Concrete, n.d. https://doi.org/10.1520/C1856_C1856M-17.
[53] ASTM C1437-15, Standard Test Method for Flow of Hydraulic Cement Mortar, ASTM International, West Conshohocken, PA, 2015, https://doi.org/10.1520/C1437-15, 2015.
[54] N. Roux, C. Andrade, M.A. Sanjuan, Experimental study of durability of reactive powder concretes, J. Mater. Civ. Eng. 8 (1996) 1–6, 10.1061/ASCE)0899-1561(1996)8:1(1).
[55] B. Graybeal, J. Tanesi, Durability of an ultrahigh-performance concrete, J. Mater. Civ. Eng. 19 (2007) 848–854, https://doi.org/10.1061/(ASCE)0899-1561, 2007) 19:10(848.
[56] D.-Y. Yoo, W. Shin, B. Chun, N. Banthia, Assessment of steel fiber corrosion in self-healed ultra-high-performance fiber-reinforced concrete and its effect on tensile performance, Cement Concr. Res. 133 (2020) 106091, https://doi.org/10.1016/j.cemconres.2020.106091.
[57] S. Abbas, A.M. Soliman, M.L. Nehdi, Exploring mechanical and durability properties of ultra-high performance concrete incorporating various steel fiber lengths and dosages, Construct. Build. Mater. 75 (2015) 429–441, https://doi.org/10.1016/j.conbuildmat.2014.11.017.
[58] D. Dobias, R. Pernicova, T. Mandlik, Water transport properties and depth of chloride penetration in ultra high performance concrete, Key Eng. Mater. 711 (2016) 137–142. https://doi.org/10.4028/www.scientific.net/KEM.711.137.
[59] O. Bonneau, M. Lachemi, E. Dallaire, J. Dugat, P.-C. Aitcin, Mechanical Properties and Durability of Two Industrial Reactive Powder Concretes, ACI Mater. J. 94 (n.d.). https://doi.org/10.14359/310.
[60] S. Kazemi, A.S. Lubell, Influence of specimen size and fiber content on mechanical properties of ultra-high-performance fiber-reinforced concrete, ACI Mater. J. 109 (2012), https://doi.org/10.14359/51684165.
[61] H. Zhang, T. Ji, X. Zeng, Z. Yang, X. Lin, Y. Liang, Mechanical behavior of ultra-high performance concrete (UHPC) using recycled fine aggregate cured under different conditions and the mechanism based on integrated microstructural parameters, Construct. Build. Mater. 192 (2018) 489–507, https://doi.org/10.1016/j.conbuildmat.2018.10.117.
[62] J. Liu, R. Guo, Applications of steel slag powder and steel slag aggregate in ultra-high performance concrete, Adv. Civ. Eng. (2018) 1426037, https://doi.org/10.1155/2018/1426037, 2018.
[63] P.P. Li, H.J.H. Brouwers, W. Chen, Q. Yu, Optimization and characterization of high-volume limestone powder in sustainable ultra-high performance concrete, Construct. Build. Mater. 242 (2020) 118112, https://doi.org/10.1016/j.conbuildmat.2020.118112.
[64] X. Wang, R. Yu, Z. Shui, Q. Song, Z. Zhang, Mix design and characteristics evaluation of an eco-friendly Ultra-High Performance Concrete incorporating recycled coral based materials, J. Clean. Prod. 165 (2017) 70–80, https://doi.org/10.1016/j.jclepro.2017.07.096.
[65] ASTM C150/C150M − 20, Standard Specification for Portland Cement, 2020, https://doi.org/10.1520/C0150_C0150M-20.
[66] QCS, Qatar General Organization for Standards and Metrology, Qatar, 2014.
[67] ASTM C127-15, Standard Test Method for Relative Density (Specific Gravity) and Absorption of Coarse Aggregate, 2015, https://doi.org/10.1520/C0127-15.
[68] ASTM D4791–19, Standard Test Method for Flat Particles, Elongated Particles, or Flat and Elongated Particles in Coarse Aggregate, (n.d.). https://doi.org/10.1520/D4791-19.

[69] ASTM C131/C131M − 20, Standard Test Method for Resistance to Degradation of Small-Size Coarse Aggregate by Abrasion and Impact in the Los Angeles Machine, 2020, https://doi.org/10.1520/C0131_C0131M-20.
[70] ASTM C88/C88M–18, Standard Test Method for Soundness of Aggregates by Use of Sodium Sulfate or Magnesium Sulfate, (n.d.). https://doi.org/10.1520/C0088_C0088M-18.
[71] L. Butler, J.S. West, S.L. Tighe, The effect of recycled concrete aggregate properties on the bond strength between RCA concrete and steel reinforcement, Cement Concr. Res. 41 (2011) 1037–1049, https://doi.org/10.1016/j.cemconres.2011.06.004.
[72] ASTM C1611/C1611M-21, Standard Test Method for Slump Flow of Self-Consolidating Concrete, 2021, https://doi.org/10.1520/C1611_C1611M-21.
[73] ASTM C39/C39M-20, Standard Test Method for Compressive Strength of Cylindrical Concrete Specimens, 2020, https://doi.org/10.1520/C0039_C0039M-20, 1–8.
[74] ASTM C1609/C1609M-12, Standard Test Method for Flexural Performance of Fiber-Reinforced Concrete (Using Beam with Third-Point Loading), 2012, https://doi.org/10.1520/C1609_C1609M-12.
[75] AASHTO TP 95, Standard Method of Test for Surface Resistivity Indication of Concrete's Ability to Resist Chloride Ion Penetration, American Association of State Highway and Transportation Officials, Washington, DC, 2011.
[76] ASTM C1202-19, Standard Test Method for Electrical Indication of Concrete's Ability to Resist Chloride Ion Penetration 1, 2019, https://doi.org/10.1520/C1202-19.
[77] ASTM C1754/C1754M-12, Standard Test Method for Density and Void Content of Hardened Pervious Concrete, 2012.
[78] A.S. El-Dieb, Mechanical, durability and microstructural characteristics of ultra-high-strength self-compacting concrete incorporating steel fibers, Mater. Des. 30 (2009) 4286–4292, https://doi.org/10.1016/j.matdes.2009.04.024.
[79] I.L. Larsen, R.T. Thorstensen, The influence of steel fibres on compressive and tensile strength of ultra high performance concrete: a review, Construct. Build. Mater. 256 (2020) 119459, https://doi.org/10.1016/j.conbuildmat.2020.119459.
[80] D.-Y. Yoo, M.J. Kim, S.-W. Kim, J.-J. Park, Development of cost effective ultra-high-performance fiber-reinforced concrete using single and hybrid steel fibers, Construct. Build. Mater. 150 (2017) 383–394, https://doi.org/10.1016/j.conbuildmat.2017.06.018.
[81] A. Abushanab, W. Alnahhal, M. Farraj, Structural performance and moment redistribution of basalt FRC continuous beams reinforced with basalt FRP bars, Eng. Struct. 240 (2021) 112390, https://doi.org/10.1016/j.engstruct.2021.112390.
[82] D.J. Kim, S.H. Park, G.S. Ryu, K.T. Koh, Comparative flexural behavior of hybrid ultra high performance fiber reinforced concrete with different macro fibers, Construct. Build. Mater. 25 (2011) 4144–4155, https://doi.org/10.1016/j.conbuildmat.2011.04.051.
[83] M. Gesoglu, E. Güneyisi, G.F. Muhyaddin, D.S. Asaad, Strain hardening ultra-high performance fiber reinforced cementitious composites: effect of fiber type and concentration, Compos. B Eng. 103 (2016) 74–83, https://doi.org/10.1016/j.compositesb.2016.08.004.
[84] W. Meng, K.H. Khayat, Effect of hybrid fibers on fresh properties, mechanical properties, and autogenous shrinkage of cost-effective UHPC, J. Mater. Civ. Eng. 30 (2018) 4018030, https://doi.org/10.1061/(ASCE)MT.1943-5533.0002212.
[85] L. Zhang, J. Liu, J. Liu, Q. Zhang, F. Han, Effect of steel fiber on flexural toughness and fracture mechanics behavior of ultrahigh-performance concrete with coarse aggregate, J. Mater. Civ. Eng. 30 (2018) 4018323, https://doi.org/10.1061/(ASCE)MT.1943-5533.0002519.
[86] R. Ma, L. Guo, S. Ye, W. Sun, J. Liu, Influence of hybrid fiber reinforcement on mechanical properties and autogenous shrinkage of an ecological UHPFRCC, J. Mater. Civ. Eng. 31 (2019), 04019032, https://doi.org/10.1061/(ASCE)MT.1943-5533.0002650.
[87] R. Kurda, J. de Brito, J.D. Silvestre, Water absorption and electrical resistivity of concrete with recycled concrete aggregates and fly ash, Cement Concr. Compos. 95 (2019) 169–182, https://doi.org/10.1016/j.cemconcomp.2018.10.004.
[88] N. Banthia, A. Bhargava, Permeability of stressed concrete and role of fiber reinforcement, ACI Mater. J. 104 (2007), https://doi.org/10.14359/18497.
[89] H. Toutanji, S. McNeil, Z. Bayasi, Chloride permeability and impact resistance of polypropylene-fiber-reinforced silica fume concrete, Cement Concr. Res. 28 (1998) 961–968, https://doi.org/10.1016/S0008-8846(98)00073-8.
[90] M.C. Rao, S.K. Bhattacharyya, S. V Barai, Influence of field recycled coarse aggregate on properties of concrete, Mater. Struct. 44 (2011) 205–220, https://doi.org/10.1617/s11527-010-9620-x.